

A Modification to the Bratseth Method
for use in Complex Terrain

David T. Myrick¹ and John D. Horel
NOAA/Cooperative Institute for Regional Prediction and
Department of Meteorology, University of Utah
Salt Lake City, UT

Steven M. Lazarus
Florida Institute of Technology
Melbourne, FL

Submitted to: *Weather and Forecasting*
February 2, 2004

1. Corresponding author address:
University of Utah
Department of Meteorology
135 South 1460 East, Rm. 819
Salt Lake City, UT 84112-0110
email: dmyrick@met.utah.edu

Abstract

An anisotropic term was added to a data assimilation system to reduce the influence across mountain barriers of corrections to the background field that are derived from surface observations. A related change was implemented to reduce the influence of observational corrections across coastal zones and land-lake boundaries. These modifications were tested using the Advanced Regional Prediction System Data Assimilation System (ADAS). Case studies are presented for two regions: the Flathead Lake region of northwest Montana and the Wasatch Front of northern Utah. The inclusion of the anisotropic term has made a modest improvement to analyses by constraining the influence of observations in mountain valleys that may differ from the weather conditions present in adjacent valleys. Rather than propagating surface weather conditions laterally through mountains, this constraint assumes that the background field remains the best choice in regions with relatively little data.

1. Introduction

Accurate objective analyses of meteorological quantities are of great importance to weather forecasters. The need for analyses of meteorological surface variables (temperature, wind, etc.) over mountainous regions for applications such as forest fire suppression, winter road maintenance, and dispersion of pollutants in urban basins is receiving increasing attention (Smith et al. 1997). These applications require data and data assimilation procedures at higher spatial resolution than is used operationally by the National Centers for Environmental Prediction (Kalnay 2003). To support higher spatial resolution analyses, mesonet observations must be incorporated that are often spaced irregularly in the horizontal and vertical (Ruggerio et al. 1996).

The research presented here relies upon analyses of meteorological variables over complex terrain that are created by the Cooperative Institute for Regional Prediction (CIRP) at the University of Utah using the Advanced Regional Prediction System (Xue et al. 2000, 2001, 2003) Data Assimilation System (ADAS, Lazarus et al. 2002). For the objective analysis, ADAS employs the Bratseth method of successive corrections (Bratseth 1986; Lazarus et al. 2002). This method was chosen over more advanced variational schemes employed by the operational centers because it is an inexpensive analysis procedure that can be run in near real-time over a large horizontal domain (western United States) at high horizontal resolution (order 2.5 km). The Bratseth method of successive corrections has been shown to converge to the same solution as optimal interpolation (Bratseth 1986; Kalnay 2003).

The irregular distribution of observations in the horizontal and vertical complicates data assimilation. This problem is exacerbated over complex terrain where the majority of the observations are located in populated valleys. Most data assimilation methods usually depend upon isotropic weights, i.e., corrections to the background field are weighted uniformly as a function of

horizontal and vertical distances between the observations and grid points. If the observations are relatively error free and their density is uniformly high throughout the analysis domain, the analysis will be constrained tightly by the observations. In this best case scenario, the resulting analysis will be able to resolve small-scale features, such as local mountain-valley circulations. However, when the data density is irregular (i.e., some subregions with high density and others with low density), the desire to resolve the local microclimate of one region may conflict with the need to relax to the background field in data void regions. This problem requires careful evaluation of the appropriate horizontal and vertical radii of influence (ROI) in a successive corrections approach or the appropriate spatial decorrelations of the background error covariance in optimal interpolation schemes.

Under certain meteorological conditions (i.e., radiational inversions in mountain valleys, cold air confined to one side of a mountain range), it may not be desirable for observational corrections to influence analysis grid points on the other side of a mountain range. Analysis methods that use isotropic weights, however, have no stipulation that controls whether corrections should propagate from one mountain valley to another. The simple solution to this problem is to reduce the ROI so that corrections are negligible between neighboring mountain valleys. However, the mountain-valley structure of the western United States is highly variable and it is impossible to select a representative ROI that works everywhere. A more complicated solution involves constraining the influence of corrections by the terrain through an anisotropic weight.

Anisotropic weighting has been proposed as a solution to various problems in the field of meteorological data assimilation in the past. Little work has been done to investigate its impact at high resolution, however, because of the computational cost to implement these methods. Endlich and Mancuso (1968) and Sasaki (1971) improved wind analyses by modifying a successive cor-

rections scheme so that greater weight was given to upwind and downwind observations compared to those in crosswind directions. Thiebaut (1976, 1977) introduced an anisotropic correlation function that improved analyses of height fields. Hessler (1984) improved analyses of surface temperature in a coastal zone by weighting spatial covariances based upon proximity to the coastline. Benjamin and Seaman (1985) tested elliptical and banana-shaped weighting functions on a curved flow field. Lazinger and Steinacker (1990) modified the observational error covariances for station pairs on opposite sides of the Alps to account for the observed sharp gradients in isentropic surfaces across the range. Miller and Benjamin (1992) describe how anisotropic functions are used to analyze potential temperature, wind and humidity in the Mesoscale Analysis and Prediction System. Otte et al. (2001) introduced synoptic-dependent anisotropic weights into the PSU-NCAR Mesoscale Model that increased forecast skill.

The primary objective of this research is to improve data assimilation methods for use in the western United States. The specific approach to be evaluated is an anisotropic modification of the Bratseth successive corrections method such that observational corrections to the background field receive less weight when the locations of the observations and grid points are separated by mountain ranges. This approach involves searching for a barrier between observation and grid point pairs. If higher terrain is found to block the path between the two points, then the weight of the observational correction upon the background field will be decreased, depending on the height of the barrier relative to a predefined scale height. In a similar manner, the observational corrections will be reduced where the observation locations and grid points are separated by coastlines. Hence, in the absence of nearby data we assume that the background field is the best choice for grid points separated by mountains or shorelines from the nearest observations.

The specifications of the University of Utah version of ADAS employed in this study are described in section 2. The anisotropic modifications to the Bratseth method of successive corrections are described in section 3. In section 4, a cross section is used to illustrate the behavior of the anisotropic term. A pair of case studies are presented in section 5 that demonstrate the utility of the anisotropic term over complex terrain. Conclusions and future work are discussed in section 6.

2. ADAS description

At CIRP, ADAS is used to generate analyses of surface meteorological variables over the western United States for a variety of applications (Lazarus et al. 2002). ADAS typically incorporates over 2,000 surface weather observations each hour from MesoWest (Horel et al. 2002). Those observations, collected from over a hundred different agencies and firms, are spaced irregularly in the horizontal and vertical; some regions have relatively high data density (e.g., northern Utah, southern Nevada, San Francisco Bay region), while others do not (e.g., northeastern Arizona). ADAS analyses have been run routinely for several years and considerable subjective experience has been gleaned with respect to both the advantages and the deficiencies of the analyses.

A few changes have been made to the Utah operational configuration of ADAS since the description provided by Lazarus et al. (2002). The background field used for the analyses has been updated from the 40 km to the 20 km version of the Rapid Update Cycle (RUC; Benjamin et al. 2002). The domain was changed to a section of the Lambert Conformal projection grid 211 utilized by the National Digital Forecast Database (NDFD; Glahn and Ruth 2003) and the analysis is now performed using a terrain data set that is consistent with that used by the NDFD. Currently, ADAS surface analyses are generated for temperature, relative humidity and wind over the western United States in near real-time at 10 (2.5) km horizontal resolution every 15 (60) minutes. The case studies presented in this paper focus on the 2.5 km resolution analyses.

The horizontal (R) and vertical (R_z) scale factors that control the ROI outlined in Table 1 of Lazarus et al. (2002) have been modified to reflect the complex distribution of stations over the western United States. The Utah operational version of ADAS varies the horizontal (vertical) scale factor from 75 km (375 m) on the first and second Bratseth passes to 50 km (250 m) on the third and fourth iterations. These scaling parameters allow the background field at most grid points to be adjusted by at least a few observations on the initial Bratseth pass while allowing the analysis to conform more closely to local observations in regions where the local data density is higher.

3. Anisotropic Modifications to ADAS

The ultimate goal of data assimilation is to interpolate observations to a regular grid. As described by Lazarus et al. (2002), the objective analysis scheme utilized by ADAS is the Bratseth method of successive corrections (Bratseth 1986). As discussed in section 1, an anisotropic factor is added to the observation-to-observation and observation-to-grid point spatial correlation functions used in the ADAS analysis. Eqs. (10) and (12) in the paper by Lazarus et al. (2002) become

$$\rho_{ij} = \exp\left(\frac{-|r_{ij}|^2}{R^2}\right) \exp\left(\frac{-|\Delta z_{ij}|^2}{R_z^2}\right) \exp\left(\frac{-|z_{oo}|^2}{R_B^2}\right) \exp(-\delta_{lw}), \quad (1)$$

$$\rho_{xj} = \exp\left(\frac{-|r_{xj}|^2}{R^2}\right) \exp\left(\frac{-|\Delta z_{xj}|^2}{R_z^2}\right) \exp\left(\frac{-|z_x - T_x|^2}{R_T^2}\right) \exp\left(\frac{-|z_{og}|^2}{R_B^2}\right) \exp(-\delta_{lw}), \quad (2)$$

where r_{ij} (r_{xj}) and Δz_{ij} (Δz_{xj}) are the horizontal and vertical distances between an observation - observation (observation - grid point) pair, z_x and T_x are the elevations of the grid point and terrain at location x , and z_{oo} (z_{og}) are the magnitude of the terrain blockage between an observation - observation (observation - grid point) pair (discussed in more detail later). The magnitude of the

spatial correlation functions depend strongly upon the values specified for R , R_z , R_T , R_B and δ_{lw} . These scaling parameters control the horizontal (R) and vertical (R_z) search radii, magnitude of the terrain factor (R_T) and the strength of the anisotropic weight (R_B) and land-water mask (δ_{lw}). The terrain factor as defined by Lazarus et al. (2002) only affects the analysis in the free atmosphere (i.e., z_x and T_x are identical when the analysis is performed at the surface).

Figure 1 shows schematically the impact of the value selected for the horizontal and vertical scaling parameters. Figure 1a depicts the horizontal plane with R set to 50 km. The black dot in the center of the figure indicates an analysis grid point and the circular rings around it represent the distance (in km) from that grid point to a nearby observation point. The arrows on the figure are labeled with the value of the horizontal (1st) term in the observation-to-grid point spatial correlation function (Eq. (2)). For example, the horizontal term in the spatial correlation function for an observation that is 50 km away will be weighted e^{-1} (63.2%) less than the observation correction for a station co-located with the grid point. A vertical cross section along the dashed line of Fig. 1a is shown in Fig. 1b. An observation that is located 750 m directly above or below the analysis grid point will be weighted the same as an observation located 75 km away in the horizontal.

In the absence of background error, the ratio of the horizontal to vertical scaling factors defines the extent to which surface observations located on the higher terrain (indicated schematically by the shading in Fig. 1a) affect the analysis at the grid point. However, without the anisotropic term in Eq. (2), surface observations located behind the terrain obstacles (hatched portions of Fig. 1a) would receive the same weight as those elsewhere that are located at the same horizontal distance from the grid point. The anisotropic term mitigates this problem by reducing the weight given to observational corrections at nearby grid points when the observation and grid point are separated by a topographic barrier. As shown in Fig. 2, the height of the terrain blockage between

an observation and a grid point (observation) is given by z_{og} (z_{oo}). As z_{og} or z_{oo} increases, the spatial correlation decreases for a given R_B (i.e., an observation on one side of a mountain has less influence upon an analysis grid point on the other side).

The spatial correlation functions (Eqs. (1) and (2)) are used to calculate the weighting terms in the successive corrections method (see Eqs. (7) and (8), Lazarus et al. 2002). The grid point and observation analysis weights, α_{xi} and α_{oi} , respectively, are dependent on the spatial correlations defined above and the ratio of observation error variance to forecast error variance, σ^2 . If the observation error variance equals zero (or is very small), then the observations are considered perfect (or nearly so) and the analysis will converge directly towards the observations. The values of σ^2 used in this study are the same as those defined in Table 2 of Lazarus et al. (2002).

An additional weighting term has been added to ADAS by simply comparing the location of the observation - observation and observation - grid point pairs. If one member of the pair is positioned over water (buoy or lake observation) and the other is not, then the value of δ_{lw} in the land-water mask term in Eqs. (1) and (2) is set to 0.5. In this manner, the corrections for observations located over water are not given as much weight over nearby land areas and vice versa. If both members of the pair are positioned over land (or water), the value of δ_{lw} is set to zero and the land-water mask term does not affect the spatial correlation.

4. Idealized Analyses

Before introducing the anisotropic weighting term into the operational version of ADAS, the term was tested using a program that applied the Bratseth scheme to a surface cross section across a mountain barrier. Results from an idealized case over the Rush and Salt Lake Valleys of northern Utah during a radiational inversion event are presented that demonstrate the behavior of the anisotropic term. The two valleys are separated by the Oquirrh Mountains and the floor of the

Rush Valley is approximately 300 m higher in elevation (Fig. 3a). For these idealized analyses, grid points were spaced 3 km apart along the horizontal axis while observations were chosen so as to mimic the actual data density shown schematically in Fig. 3a (i.e., the data density is low along the west slope of the Salt Lake Valley). The horizontal (vertical) scaling factor for these analyses was set to 75 km (375 m) for the first and second passes and 50 km (250 m) for eight additional iterations. Two different background fields were used to demonstrate the sensitivity of the analysis to the quality of the initial state. The observation error variance-to-forecast error variance, σ^2 was set to 0.1. For the purposes of this paper, negative (positive) differences between an observation and the analysis value at the observation location (i.e., when an observation is colder (warmer) than the analysis value) will result in a negative (positive) correction for that observation at a nearby analysis grid point. On the initial pass, the analysis value is given by the background field.

The impact of the anisotropic weight upon the analysis using a poor background field is shown in Fig. 3b. The background field used for this case does not capture the pooling of cold air at the floor of the Rush and Salt Lake Valleys or the higher temperatures along the valley side-walls. The greatest difference between the isotropic and anisotropic analysis occurs along the data sparse west slope of the Salt Lake Valley at a horizontal distance of approximately 50 km. The isotropic analysis at this point is more than 3°C colder than the anisotropic analysis. The colder isotropic analysis along the west slope is created by negative corrections from the cold observations along the floor of the Rush Valley at approximately the same elevation. The impact of the cold Rush Valley observations along the west slope is reduced by the anisotropic term. This constraint forces the temperature analysis along the west slope to be derived mostly from observations located within the Salt Lake Valley, rather than from data on the other side of the Oquirrh Mountains where the temperature structure is significantly different.

The impact of the anisotropic term on the analysis strongly depends on the quality of the background field. Anisotropic and isotropic analyses for a background field of high quality is shown in Fig. 3c. The analyses are nearly identical, except along the west slope. The isotropic analysis at higher elevations (at horizontal distances of 30-40 km) is slightly warmer because positive corrections from observations at the same elevation can pass through the Oquirrh Mountains. At lower elevations (at horizontal distances of 45-55 km), the anisotropic analysis is warmer because the negative corrections from Rush Valley observations are minimized, allowing the positive corrections from observations on the east bench to dominate.

5. Results

Sample ADAS analyses are now presented to demonstrate the effect of the anisotropic term over the western United States. Two subdomains are evaluated: the Wasatch Front of northern Utah and the Flathead Lake region of northwest Montana. The 2.5 km resolution terrain used in these analyses is shown in Fig. 4 and a close-up of the Wasatch Front terrain is shown in Fig. 5.

As was shown in section 4, the magnitude of the change resulting from the implementation of the anisotropic term is directly related to the quality of the background field. Experience using the RUC as a background field for ADAS has shown that when the boundary layer is well mixed (i.e., in the vicinity of convection or synoptic-scale frontal zones), the impact of the anisotropic term is minimal on an analysis. An example anisotropic ADAS analysis of a synoptic-scale cold front near the Wasatch Front is shown in Fig. 6. Differences between the anisotropic analysis (Fig. 6) and the isotropic case (not shown) are small because the boundary layer at this time was well mixed and the RUC background field captured the structure and position of the surface cold front. However when the atmospheric boundary layer is not well mixed (e.g, in mountain valleys during early morning radiational inversions), the impact of the anisotropic term is more pro-

nounced because the RUC background has trouble resolving local mesoscale structures in steep mountain valleys. Because the magnitude of the change resulting from the anisotropic term is small to begin with, we purposely show cases in this paper where the RUC background field has a difficult time resolving localized mesoscale features. It is under these circumstances that the greatest variation between the anisotropic and isotropic analyses occurs.

a. Wasatch Front

The analyses presented in this section are for a radiational inversion event at 1300 UTC 10 April 2003 for a portion of the Wasatch Front domain outlined by the black box in Fig. 5. The analyses utilize the current University of Utah operational ADAS settings for R and R_z and the anisotropic factor R_B is set to 500 m. The land-water mask described earlier is also implemented in these analyses. Presented are the RUC, isotropic ADAS and anisotropic ADAS analyses of temperature ($^{\circ}\text{C}$) and the difference between the anisotropic and isotropic ADAS analyses in a four panel chart (Fig. 7). A surface cross section of temperature ($^{\circ}\text{C}$) (Fig. 8) along line segment AB in Fig. 5 is also presented to aid in comparisons.

The RUC background field (Fig. 7a) for this case is unable to capture the mesoscale temperature structure of the Salt Lake, Rush and Tooele Valleys. A close inspection of the surface observations (Fig. 7a) shows temperatures on the benches of the Salt Lake Valley are about 3°C higher than the observations on valley floor (i.e., an inverted temperature profile along the slope). Comparing the RUC temperature analysis (Fig. 7a) to the plotted observations, it is apparent that the RUC analysis is too warm. The RUC was also unable to resolve the inverted temperature structure that existed between the valley floors and benches (Fig. 8).

By introducing mesonet observations, the ADAS analyses were able to capture mesoscale temperature structures. The isotropic and anisotropic ADAS analyses (Figs. 7b and 7c) resolved

the colder temperatures in the Rush Valley and are more representative of the observations in the Salt Lake Valley than the RUC analysis. The surface cross section (Fig. 8) also indicates that the ADAS analyses have captured the warmer temperatures near the east bench of the Salt Lake Valley and on the east slope of the Rush Valley at horizontal distances of 80 and 20 km, respectively. The isotropic analysis (Fig. 7b) however, has trouble analyzing the higher temperatures along the west slope compared to those on the valley floor. From the surface cross section (Fig. 8), it is apparent that the isotropic case analyzes the temperature along the west slope to be near 7°C, while the observations indicate a temperature of 11-13°C. As was discussed in section 4, this cold bias on the west slope is caused in part by negative corrections from cold observations in the Rush Valley propagating through the Oquirrh Mountains.

The effect of the anisotropic term can be seen in the difference plot between the anisotropic and isotropic analyses (Fig. 7d) and the surface cross section (Fig. 8). Along the west slope, the anisotropic ADAS analysis is approximately 1°C warmer (Fig. 8) than the isotropic case. Negative corrections from the cold observations in the Rush Valley are no longer able to propagate through the Oquirrh Mountains. The opposing effect can be seen in the Rush Valley. The anisotropic analysis is approximately 1°C colder because positive observation corrections from the Salt Lake Valley are reduced.

The magnitude of the change between the anisotropic and isotropic analyses is relatively small (on the order of 0.5-1.5°C) over most of the Wasatch Front region (Figs. 7d and 8). This small change over the Wasatch Front is due to the large number of observations in northern Utah (observations in Fig. 7 have been filtered for clarity). An example of a region where the anisotropic term has a significant impact upon the analysis is over the Skull Valley. The anisotropic analysis restricts the passage of negative corrections from the data dense Tooele and Rush Valleys to the

east. As a result, the anisotropic analysis over the Skull Valley is warmer (Fig. 7d) because it is driven mostly by the warm RUC background field.

The four-panel chart in Fig. 7 also demonstrates the utility of the land-water mask. Temperature observations over the Great Salt Lake at this time were near 10°C while valley level observations surrounding the lake averaged 2°C colder. The isotropic temperature analysis (Fig. 7b) was influenced by these colder observations, especially over the northeast corner of the lake where temperatures were analyzed to be 6-10°C. The inclusion of the land-water mask however, reduced the propagation of negative corrections from land stations over the lake and vice versa. The resulting anisotropic ADAS temperature analysis (Fig. 7c) over the Great Salt Lake is a better reflection of the observations over the lake and the background field.

b. Flathead Lake

The 2.5 km terrain for the Flathead Lake region is shown in Fig. 9. We present this region because a data dense valley (the Flathead Valley) is located adjacent to valleys with few or no observations (e.g., the Swan River Valley). The results presented utilize horizontal and vertical scaling factors that differ from the Wasatch Front case and do not include the land-water mask. The horizontal (vertical) scale factor was set to 75 km (750 m) for the first two passes and to 50 km (500 m) for the final two Bratseth iterations. A broader vertical scaling parameter was used in this case because there is significant vertical separation of observations in this region. A calculation of the distance between each observation and the nearest grid point found that for northwest Montana, the average vertical separation between each observation and the closest neighboring grid point is 212 m while over northern Utah it is 151 m. Vertical separations greater than 500 m were neglected in these calculations so that these values did not become inflated by observation - grid point pairs that have separations well outside the vertical radius of influence.

Similar to the Wasatch Front case, a four panel chart (Fig. 10) and a surface cross section (Fig. 11) along line segment CD in Fig. 9 are presented for 0800 UTC 20 March 2003 over the Flathead Lake region. A close inspection of the surface observations indicates that the RUC background field (Fig. 10a) for this case was too warm over the valleys. Temperatures over the Flathead Valley ranged from -4 to 1°C while the RUC analyzed temperatures greater than 4°C.

The isotropic ADAS analysis (Fig. 9b) is colder and more representative of the surface observations in the Flathead Valley than the RUC analysis. The isotropic analysis (Fig. 9b) also propagates negative observation corrections from the Flathead Valley to nearby data sparse valleys. For example, the isotropic ADAS temperature analysis over the Swan River Valley is highly dependent upon observational corrections from the Flathead Valley because these two valleys are located within the scope of the horizontal and vertical radii of influence.

The anisotropic ADAS analysis (Fig. 10c) restricts the passage of observational corrections through the Mission Range. The resulting analysis over the Swan River Valley is about 3°C warmer (Fig. 11). By losing the negative corrections from the Flathead Valley, the anisotropic ADAS analysis over the Swan River Valley is driven mostly by the RUC background. The anisotropic analysis over the southern portion of the Flathead Valley is approximately 1.5°C colder (Fig. 11) because positive observational corrections from stations to the south and southwest (not shown) are reduced.

Figures 9c and 9d illustrate a problem associated with the terrain search routine added to ADAS to calculate z_{oo} and z_{og} . In the northern Flathead Valley near Kalispell, a narrow zone of colder temperatures is analyzed horizontally across the valley. This analysis feature is created by the observation at Hungry Horse (elevation 983 m), which is located between the Whitefish and Swan Ranges. The temperature at Hungry Horse (-3°C) is a few degrees colder than the observa-

tions in the northern Flathead Valley. Since this observation is at a comparable elevation and is not blocked by the mountains, negative corrections are able to propagate through the narrow terrain opening and affect grid points located directly to the west in the Flathead Valley.

6. Discussion and Future Work

An anisotropic modification to the Bratseth method of successive corrections has been introduced that reduces the spread of observational corrections laterally through terrain in an effort to improve meteorological analyses in mountainous regions. A related modification was made to reduce the influence of observational corrections from stations over water to surrounding land areas and vice versa. ADAS analyses over the Flathead Lake region of northwest Montana and the Wasatch Front of northern Utah were used to illustrate the utility of the anisotropic modifications and some of its limitations.

The effects of the anisotropic term and land-water mask upon the analyses varies from location to location. In a valley with abundant observations, mesoscale structures (i.e. inverted temperatures along the valley sidewalls) are more likely to be analyzed better because observations within the valley are weighted more heavily relative to observations outside the valley. In a data sparse valley, however, there is a greater dependence upon the background field because observational corrections from nearby valleys are reduced. This may be favorable if the background field is of high quality or during situations where the structure of adjacent valleys is different; however if the background field is poor or the boundary layer is well mixed, the spreading of corrections from one valley to another may be beneficial. Similar arguments can be posed regarding the land-water anisotropic mask. Improvement is evident in analyses with observations located over both the land and water. However, in areas where observations are only present over

the land, the quality of the analysis over water is strongly tied to the accuracy of the background field.

The method presented to reduce the propagation of corrections through topographic blockages has limitations. In the Flathead Valley analyses (see Figs. 9c and 9d), a narrow zone of colder temperatures was analyzed near Kalispell because negative observational corrections leaked westward through a narrow gap in the mountains. To correct this problem, a search for terrain beyond simply the most direct route between two points could be implemented.

The implementation of the anisotropic term has helped to identify appropriate horizontal and vertical scaling parameters. To obtain greater detail in data dense valleys, a short horizontal search radius could be used to remove the influence of distant non-representative observations. However, using this approach jeopardizes the analysis quality in data sparse areas because a short ROI creates a noisy analysis (bull's eyes) near isolated observations that differ from the background field (Lu and Browning 1998; Kalnay 2003). The anisotropic term, however, allows ADAS to maintain a relatively large horizontal search radius while constricting observational corrections by the terrain. The selection of a representative vertical scaling factor remains a challenge because there are fewer observations at higher elevations and the vertical separation between stations varies widely.

The addition of the anisotropic term has led to a modest improvement in the ADAS analyses over complex terrain. Further improvement is dependent primarily on three factors: 1) obtaining more representative surface observations in data sparse areas, 2) improving the background field, and 3) improving the analysis methodology. Since the anisotropic term constrains corrections by the terrain, the addition of more observing sites in remote locations will help to improve the analysis. As was seen in the case studies in section 5, the RUC background field does not

resolve the inverted temperature field often observed during the night and early morning along the slopes of steep mountain valleys. The approach used here to make corrections to the RUC background could be improved by using a data assimilation system that employs the same model for the background field and the analysis. Possible improvements to the analysis methodology include posterior filtering techniques outlined by Pedder (1993) and Ioannidou and Pedder (1999) and extending the ideas described by Lazarus et al. (2002), in which the wind and mass fields are constrained to be dynamically consistent.

Acknowledgements. The authors would like to thank Eugene Petrescu for providing the NDFD terrain data and his comments on this research. This work was supported by the U.S. Department of Energy grant DEFG0300ER62841 and NOAA grant NA77WA0572 to the NOAA Cooperative Institute for Regional Prediction at the University of Utah. This study was made possible in part due to the data made available by the governmental agencies, commercial firms, and educational institutions participating in MesoWest.

References

- Benjamin, S. G., and N. L. Seaman, 1985: A simple scheme for objective analysis in curved flow. *Mon. Wea. Rev.*, **113**, 1184-1198.
- , and Coauthors, 2002: RUC20 - The 20-km version of the Rapid Update Cycle. NWS Tech. Procedures Bulletin No. 490. NOAA/NWS, 30 pp. [National Weather Service, Office of Meteorology, 1325 East-West Highway, Silver Spring, MD 20910] (Available online at <http://205.156.54.206/om/tpb/490.htm>).
- Bratseth, A. M., 1986: Statistical interpolation by means of successive corrections. *Tellus*, **38**(A), 439-447.
- Endlich, R. M., and L. Mancuso, 1968: Objective analysis of environmental conditions associated with severe thunderstorms and tornadoes. *Mon. Wea. Rev.*, **96**, 342-350.
- Glahn, H. R., D. P. Ruth, 2003: The new digital forecast database of the National Weather Service. *Bull. Amer. Meteor. Soc.*, **84**, 195-201.
- Hessler, G., 1984: Experiments with statistical objective analysis techniques for representing a coastal surface temperature field. *Bound.-Layer Meteor.*, **28**, 375-389.

- Horel, J., and Coauthors, 2002: Mesowest: Cooperative mesonets in the western United States. *Bull. Amer. Meteor. Soc.*, **83**, 211-226.
- Ioannidou, L, and M. A. Pedder, 1999: Three-dimensional applications of a successive corrections analysis scheme to mesoscale observations. *Mon. Wea. Rev.*, **127**, 236-251.
- Kalnay, E., 2003: *Atmospheric Modeling, Data Assimilation and Predictability*. Cambridge University Press, 341 pp.
- Lanzinger, A., and R. Steinacker, 1990: A fine mesh analysis scheme designed for mountainous terrain. *Meteor. Atmos. Phys.*, **43**, 213-219.
- Lazarus, S. M., C. M. Ciliberti, J. D. Horel and K. A. Brewster, 2002: Near-real-time applications of a mesoscale analysis system to complex terrain. *Wea. Forecasting.*, **17**, 971-1000.
- Lu, C. and G. L. Browning, 1998: The impact of observational errors on objective analysis. *J. Atmos. Sci.*, **55**, 1791-1807.
- Miller, P. A., and S. G. Benjamin, 1992: A system for the hourly assimilation of surface observations in mountainous and flat terrain. *Mon. Wea. Rev.*, **120**, 2342-2359.
- Otte, T. L., 2001: A heuristic study of the importance of anisotropic error distributions in data assimilation. *Mon. Wea. Rev.*, **129**, 766-783.

- Pedder, M. A., 1993: Interpolation and filtering of spatial observations using successive corrections and Gaussian filters. *Mon. Wea. Rev.*, **121**, 2889-2902.
- Ruggiero, F. H., K. D. Sashegyi., R. V. Madala, and S. Raman, 1996: The use of surface observations in four-dimensional data assimilation using a mesoscale model. *Mon. Wea. Rev.*, **124**, 1018-1033.
- Sasaki, Y., 1971: A theoretical interpretation of anisotropically weighted smoothing on the basis of numerical variational analysis. *Mon. Wea. Rev.*, **99**, 698-707.
- Smith, R., and Coauthors, 1997: Local and remote effects of mountains on weather: research needs and opportunities. *Bull. Amer. Meteor. Soc.*, **78**, 877-892.
- Thiebaut, H. J., 1976: Anisotropic correlation functions for objective analysis. *Mon. Wea. Rev.*, **104**, 994-1002.
- , 1977: Extending estimation accuracy with anisotropic interpolation. *Mon. Wea. Rev.*, **105**, 691-699.
- Xue, M., K. K. Droegemeier, and V. Wong, 2000: The Advanced Regional Prediction System (ARPS) - A multiscale nonhydrostatic atmospheric simulation and prediction model. Part I: Model dynamics and verification. *Meteor. Atmos. Phys.*, **75**, 161-193.

-----, and Coauthors, 2001: The Advanced Regional Prediction System (ARPS) - A multiscale nonhydrostatic atmospheric simulation and prediction tool. Part II: Model physics and applications. *Meteor. Atmos. Phys.*, **76**, 143-165.

-----, D. Wang, J. Gao, K. Brewster, and K. K. Droegemeier, 2003: The Advanced Regional Prediction System (ARPS), storm-scale numerical weather prediction and data assimilation. *Meteor. Atmos. Phys.*, **82**, 139-170.

Figure Captions

Figure 1: Schematic of the horizontal (a) and vertical (b) distribution of spatial correlation between a grid point and nearby observation. The horizontal and vertical scale factors are equal to 50 km and 500 m, respectively. Shaded regions in (a) depict higher terrain and hatched regions indicate areas where observations are blocked by the terrain. Ellipses of equal correlation are not drawn to scale in (b).

Figure 2: Schematic of analysis grid points (filled circles) and observations (open circles). The height of the intervening terrain for an observation - observation pair (z_{oo}) and observation - grid point pair (z_{og}) is shown.

Figure 3: Anisotropic and isotropic analyses using the Bratseth method for a surface cross section located over the Wasatch Front; (a) terrain height (km) vs. horizontal distance (km), (b) analysis of temperature ($^{\circ}\text{C}$) for a poor background field, (c) analysis of temperature ($^{\circ}\text{C}$) for a good background field.

Figure 4: Surface terrain (m, shaded according to scale) for the western United States at 2.5 km resolution. Terrain considered water in the land-water masking is shaded black. The Wasatch Front and the Flathead Lake region are denoted by black boxes labeled WF and FL, respectively.

Figure 5: Surface terrain (m, shaded according to scale), county boundaries (dashed black lines), and bodies of water (solid black lines) for the Wasatch Front (indicated by the box labeled WF in

Fig. 4) at 2.5 km resolution. Terrain considered water in the land-water masking is shaded black. The black box denotes the subdomain examined later in Fig. 7 and line segment AB denotes the terrain cross section described later in Fig. 8.

Figure 6: Wasatch Front ADAS analysis of temperature ($^{\circ}\text{C}$) for 1900 UTC 2 April 2003. Surface stations (indicated by + symbols) are annotated with observations of temperature ($^{\circ}\text{C}$) and winds [full (half) barb denote 10 (5) m s^{-1}].

Figure 7: Wasatch Front region (a) RUC, (b) isotropic ADAS and (c) anisotropic ADAS analyses of temperature ($^{\circ}\text{C}$) for 1300 UTC 10 April 2003. (d) Difference in temperature ($^{\circ}\text{C}$) between anisotropic (c) and isotropic (b) ADAS analyses. Surface stations (indicated by + symbols) are annotated with observations of temperature ($^{\circ}\text{C}$) and winds [full (half) barb denote 10 (5) m s^{-1}]. The locations of the Rush, Salt Lake, Skull and Tooele Valleys are indicated by R, S, Sk and T, respectively.

Figure 8: Terrain cross section along line segment AB in Fig. 5 for anisotropic ADAS, isotropic ADAS and RUC background analyses of temperature ($^{\circ}\text{C}$) at 1300 UTC 10 April 2003.

Figure 9: Same as in Fig. 5 but for the Flathead Lake region. Station locations are indicated by a plus sign (+). The opening of a narrow river valley to the northeast of Kalispell is denoted by the small black arrow. Line segment CD denotes the terrain cross section described later in Fig. 11.

Figure 10: Same as in Fig. 7 but for the Flathead Lake region at 0800 UTC 20 March 2003. The locations of the Flathead and Swan Valleys are indicated by F and S, respectively. The opening of a narrow river valley to the northeast of Kalispell, MT is denoted by a small black arrow.

Figure 11: Same as Fig. 8 but for line segment CD in Fig. 9 at 0800 UTC 20 March 2003. Black diamonds denote temperature ($^{\circ}\text{C}$) observations located within 20 km of the cross section.

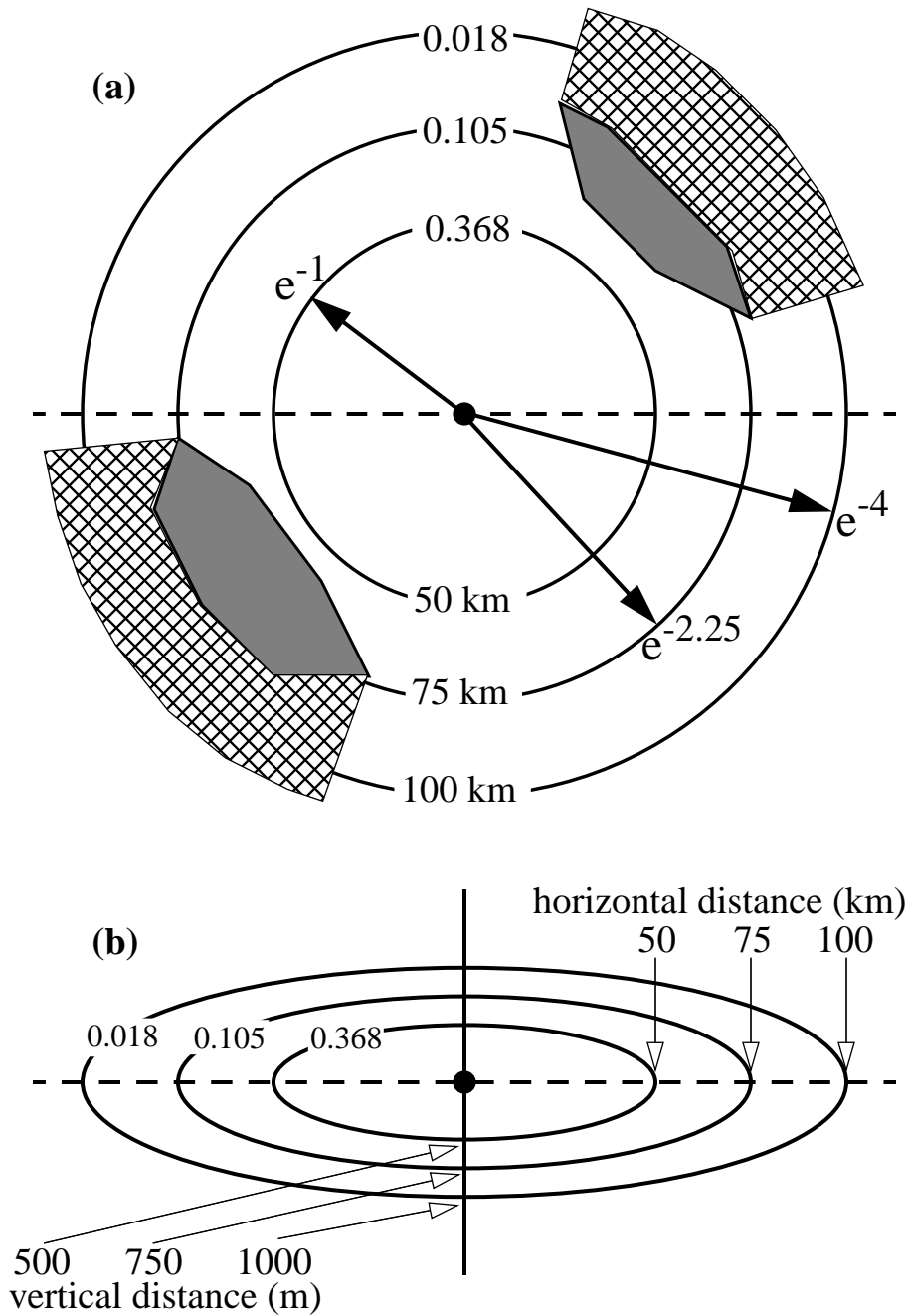


Figure 1: Schematic of the horizontal (a) and vertical (b) distribution of spatial correlation between a grid point and nearby observation. The horizontal and vertical scale factors are equal to 50 km and 500 m, respectively. Shaded regions in (a) depict higher terrain and hatched regions indicate areas where observations are blocked by the terrain. Ellipses of equal correlation are not drawn to scale in (b).

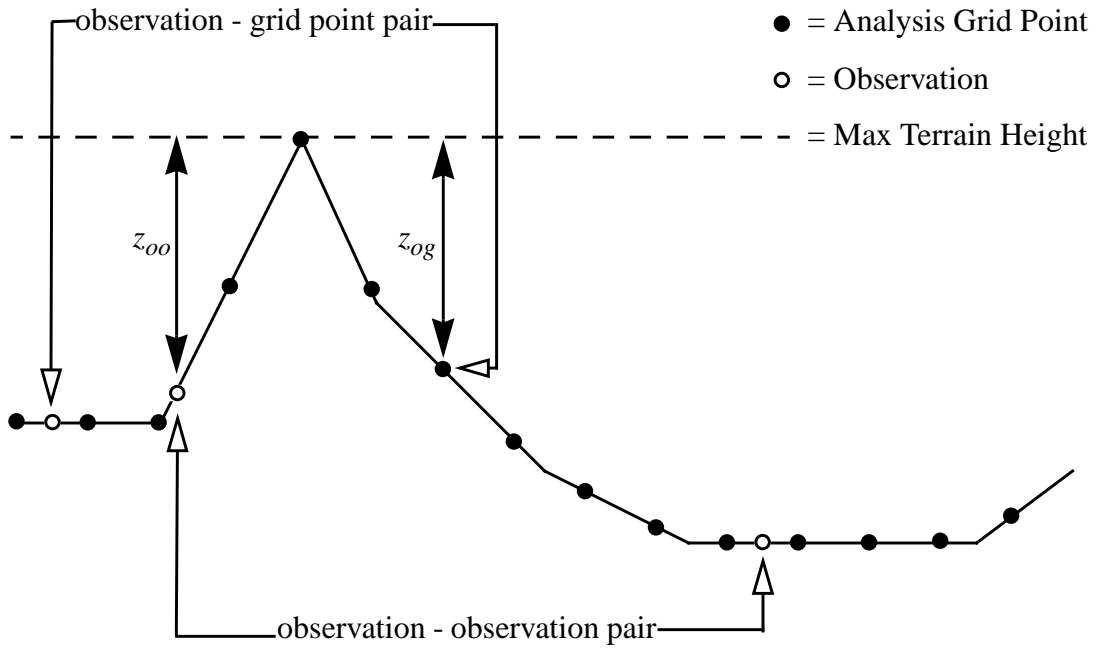


Figure 2: Schematic of analysis grid points (filled circles) and observations (open circles). The height of the intervening terrain for an observation - observation pair (z_{oo}) and observation - grid point pair (z_{og}) is shown.

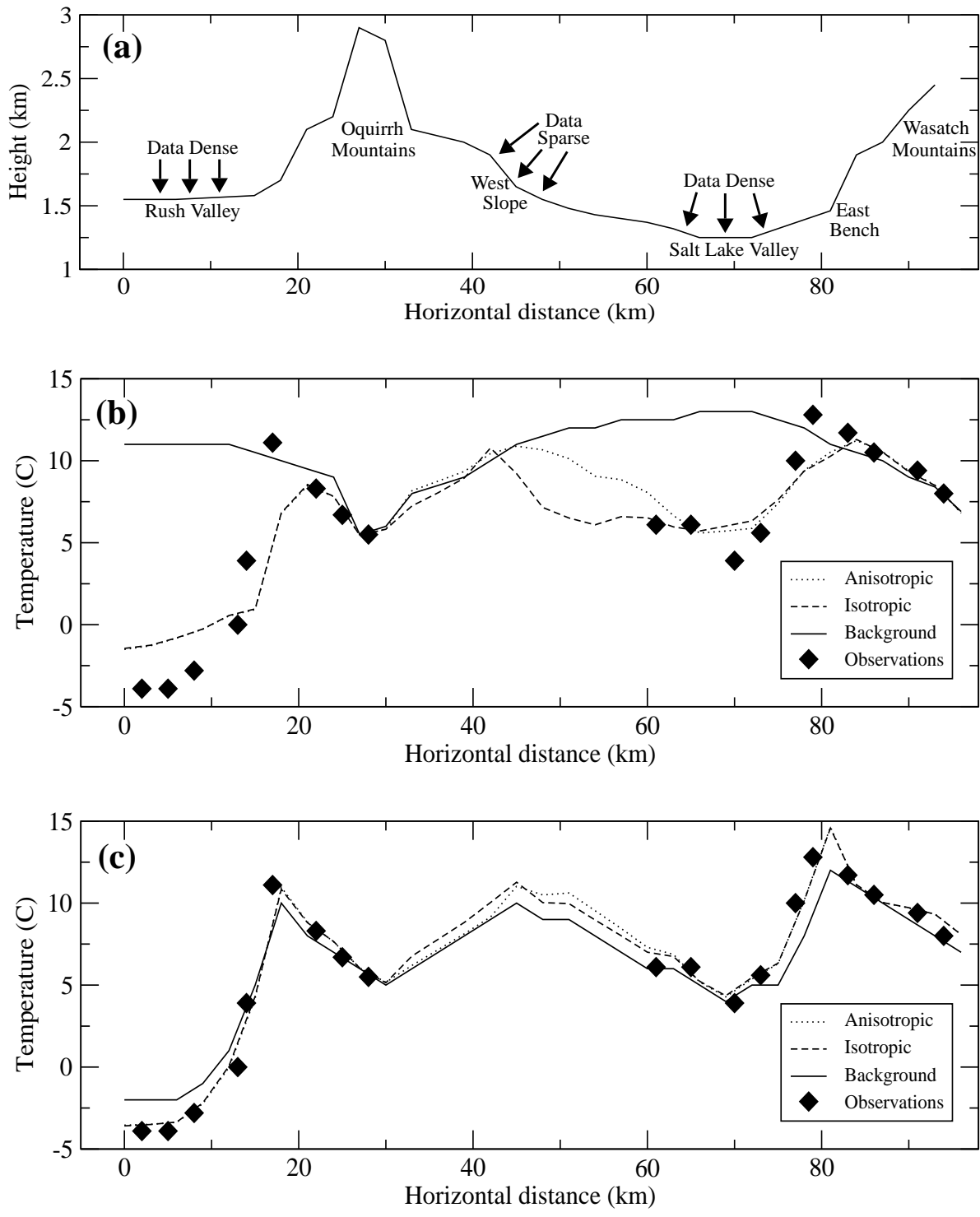


Figure 3: Anisotropic and isotropic analyses using the Bratseth method for a surface cross section located over the Wasatch Front; (a) terrain height (km) vs. horizontal distance (km), (b) analysis of temperature (°C) for a poor background field, (c) analysis of temperature (°C) for a good background field.

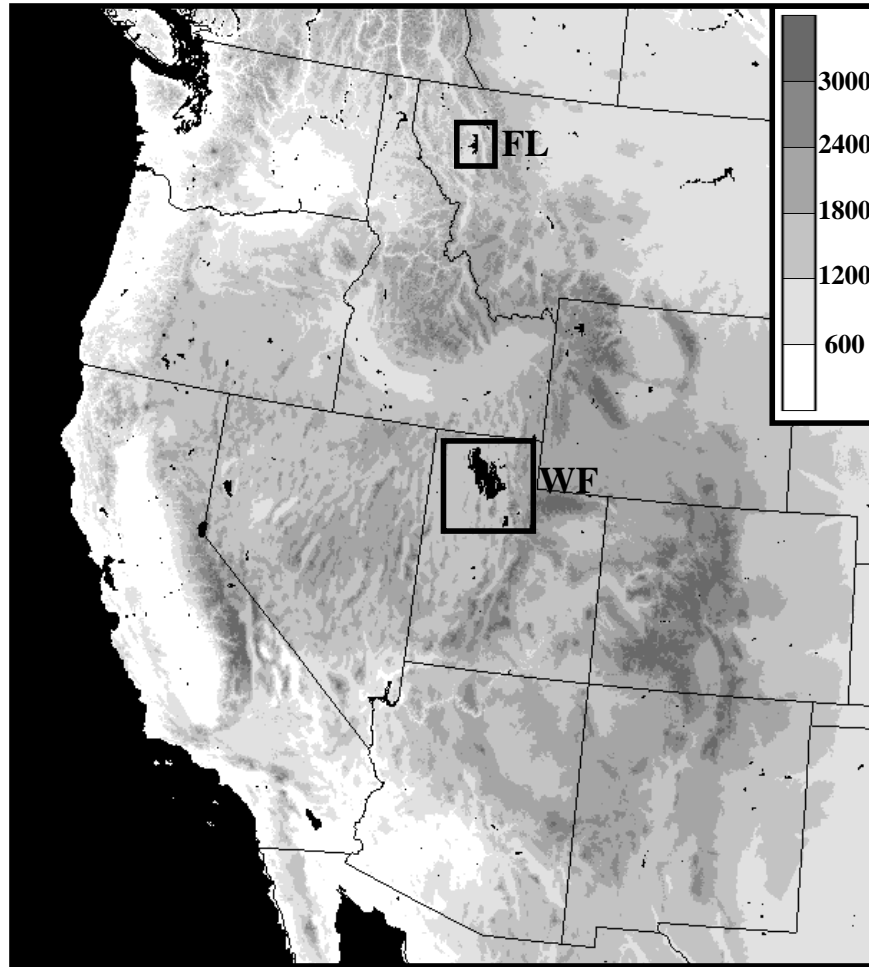


Figure 4: Surface terrain (m, shaded according to scale) for the western United States at 2.5 km resolution. Terrain considered water in the land-water masking is shaded black. The Wasatch Front and the Flathead Lake region are denoted by black boxes and labeled WF and FL, respectively.

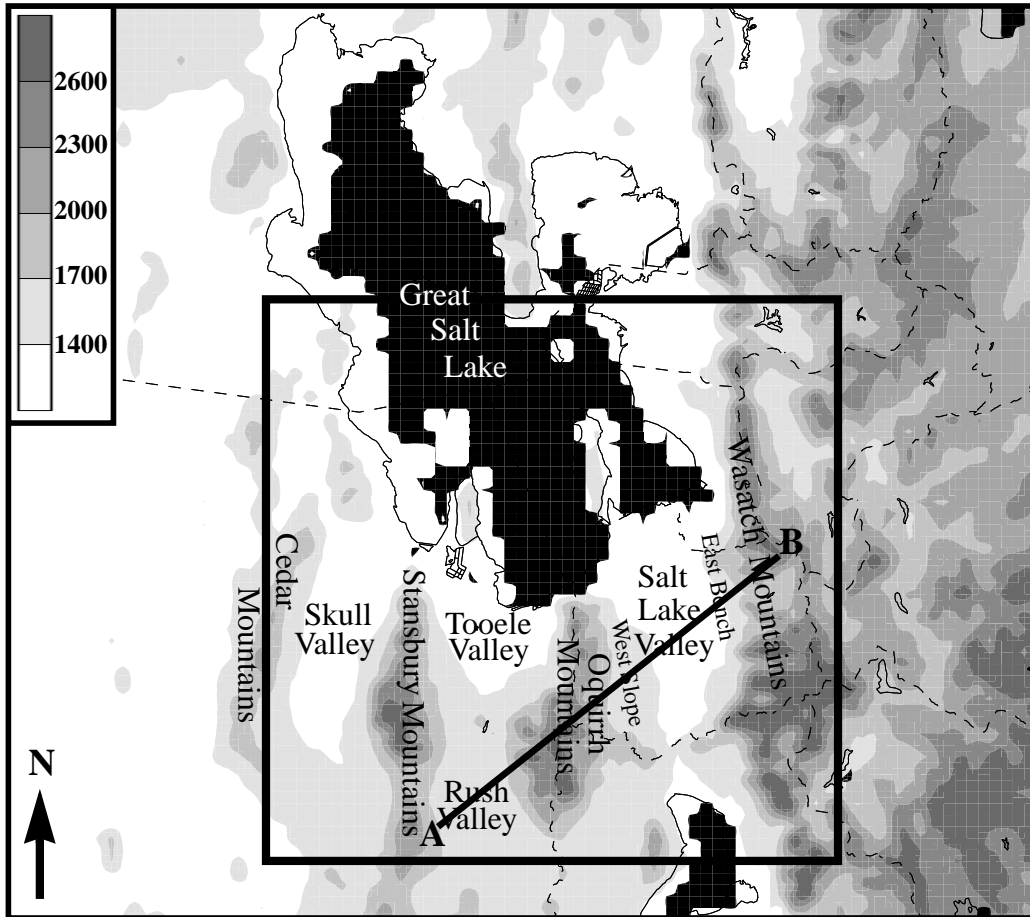


Figure 5: Surface terrain (m, shaded according to scale), county boundaries (dashed black lines), and bodies of water (solid black lines) for the Wasatch Front (indicated by the box labeled WF in Fig. 4) at 2.5 km resolution. Terrain considered water in the land-water masking is shaded black. The black box denotes the subdomain examined later in Fig. 7 and line segment AB denotes the terrain cross section described later in Fig. 8.

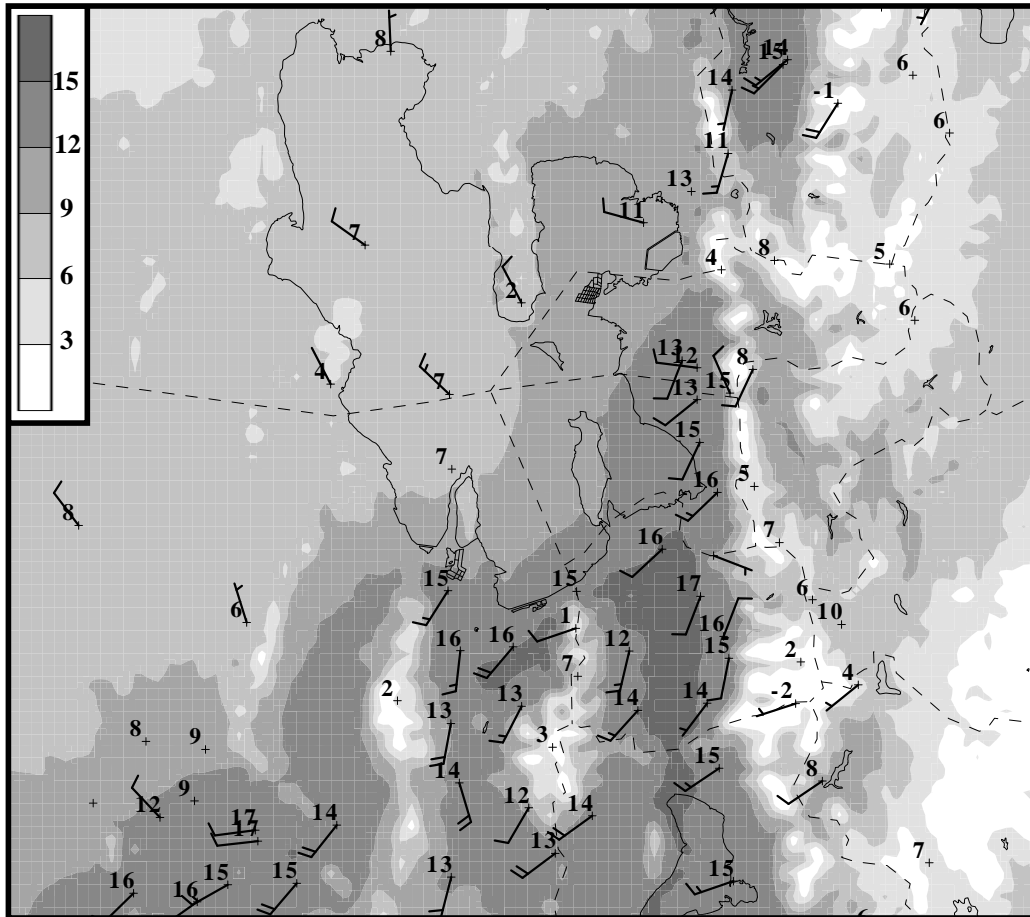


Figure 6: Wasatch Front ADAS analysis of temperature ($^{\circ}\text{C}$) for 1900 UTC 2 April 2003. Surface stations (indicated by + symbols) are annotated with observations of temperature ($^{\circ}\text{C}$) and winds [full (half) barb denote 10 (5) m s^{-1}].

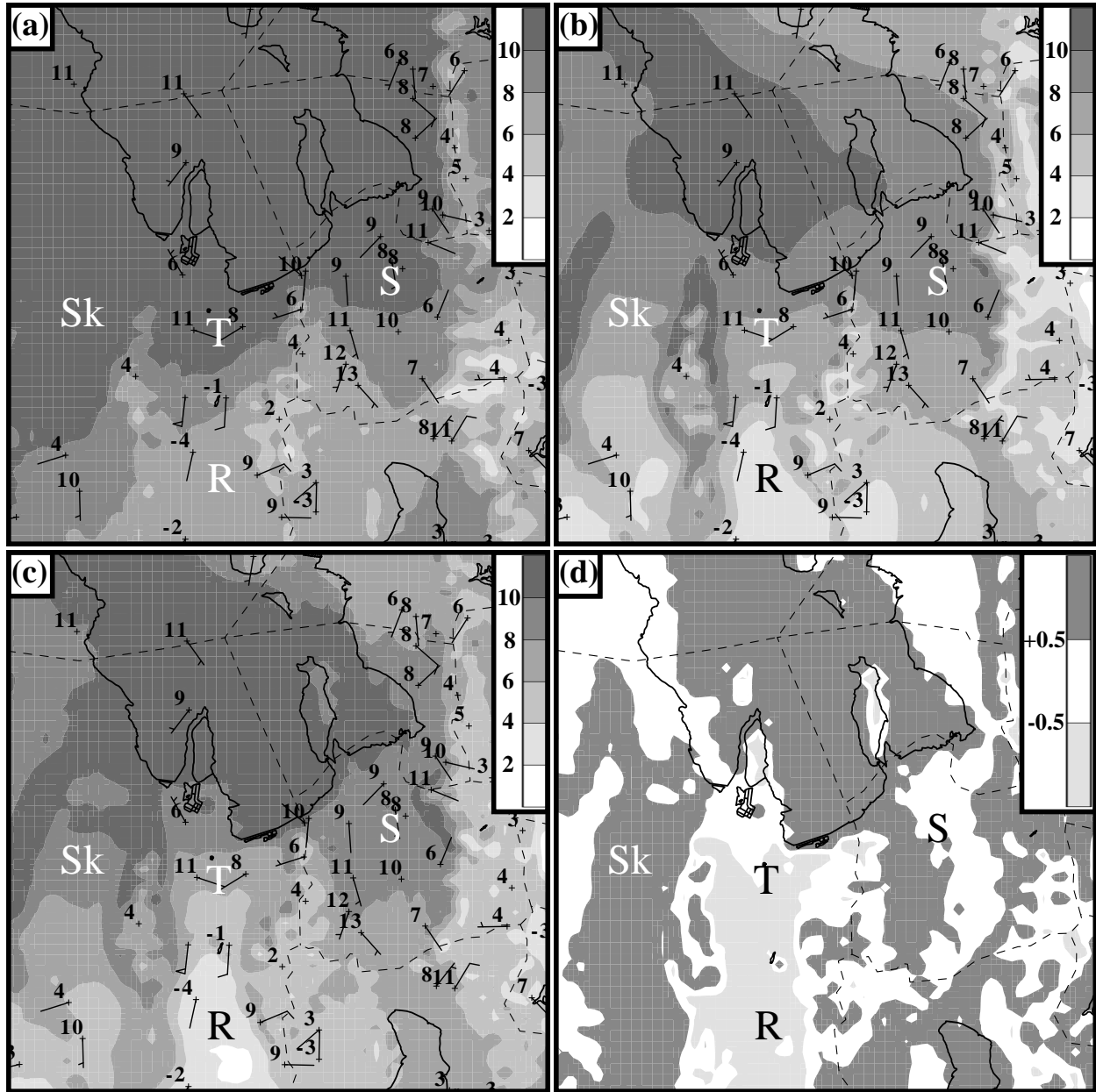


Figure 7: Wasatch Front region (a) RUC, (b) isotropic ADAS and (c) anisotropic ADAS analyses of temperature ($^{\circ}\text{C}$) for 1300 UTC 10 April 2003. (d) Difference in temperature ($^{\circ}\text{C}$) between anisotropic (c) and isotropic (b) ADAS analyses. Surface stations (indicated by + symbols) are annotated with observations of temperature ($^{\circ}\text{C}$) and winds [full (half) barb denote 10 (5) m s^{-1}]. The locations of the Rush, Salt Lake, Skull and Tooele Valleys are indicated by R, S, Sk and T, respectively.

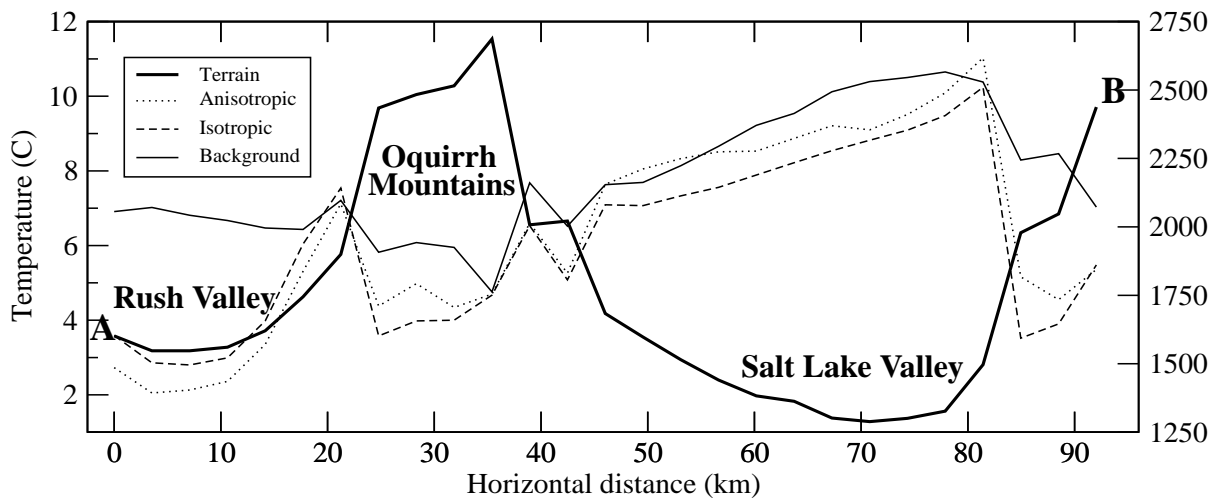


Figure 8: Terrain cross section along line segment AB in Fig. 5 for anisotropic ADAS, isotropic ADAS and RUC background analyses of temperature ($^{\circ}\text{C}$) at 1300 UTC 10 April 2003.

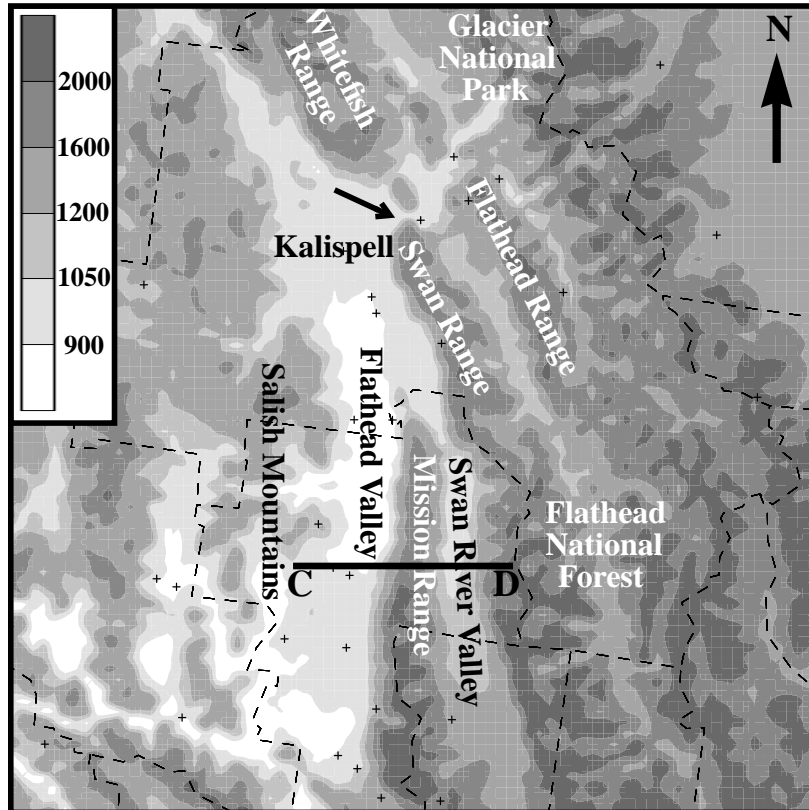


Figure 9: Same as Fig. 5 but for the Flathead Lake region. Station locations are indicated by a plus sign (+). The opening of a narrow river valley to the northeast of Kalispell is denoted by the small black arrow. Line segment CD denotes the terrain cross section described later in Fig. 11.

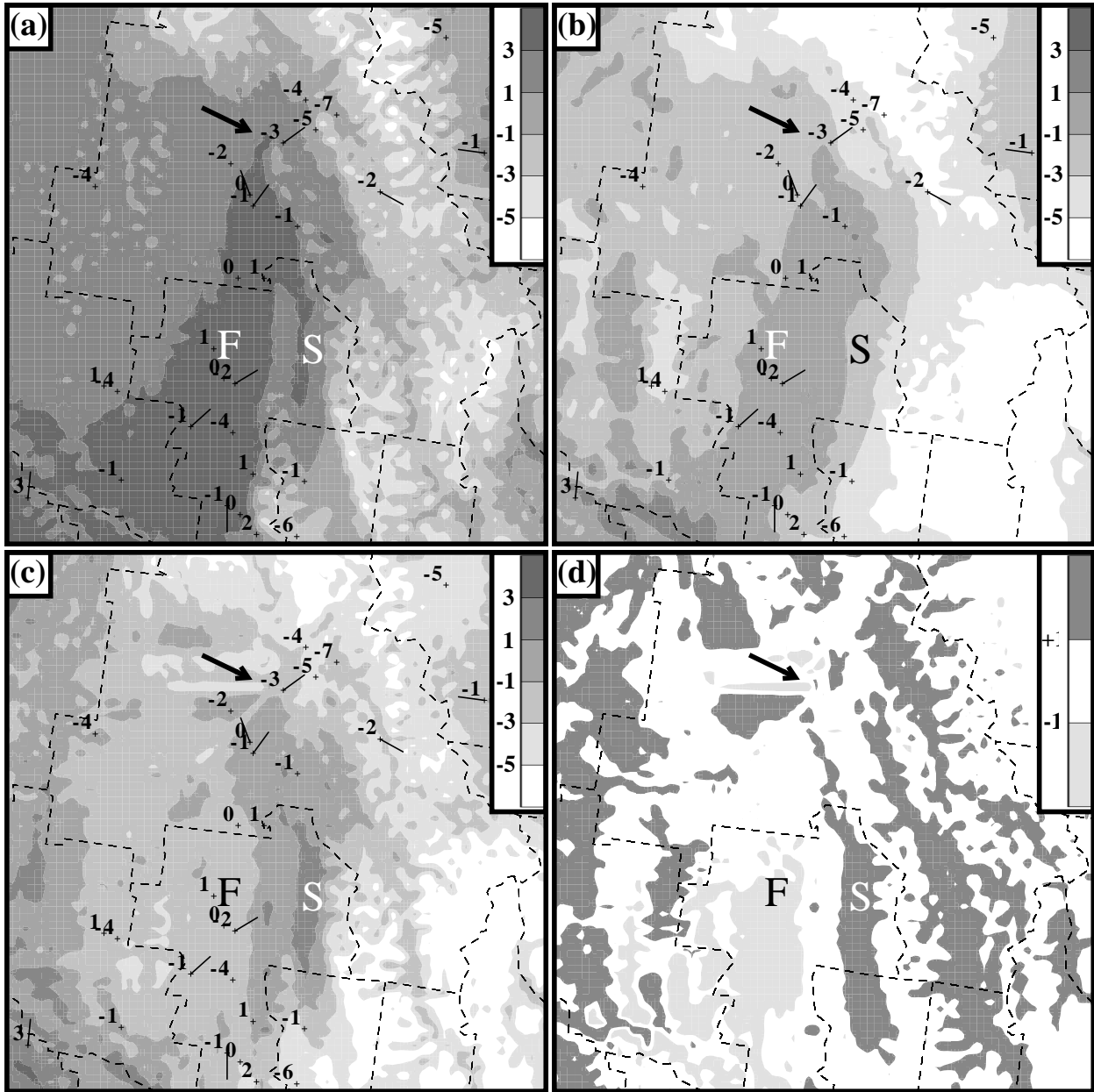


Figure 10: Same as in Fig. 7 but for the Flathead Lake region at 0800 UTC 20 March 2003. The locations of the Flathead and Swan Valleys are indicated by F and S, respectively. The opening of a narrow river valley to the northeast of Kalispell, MT is denoted by a small black arrow.

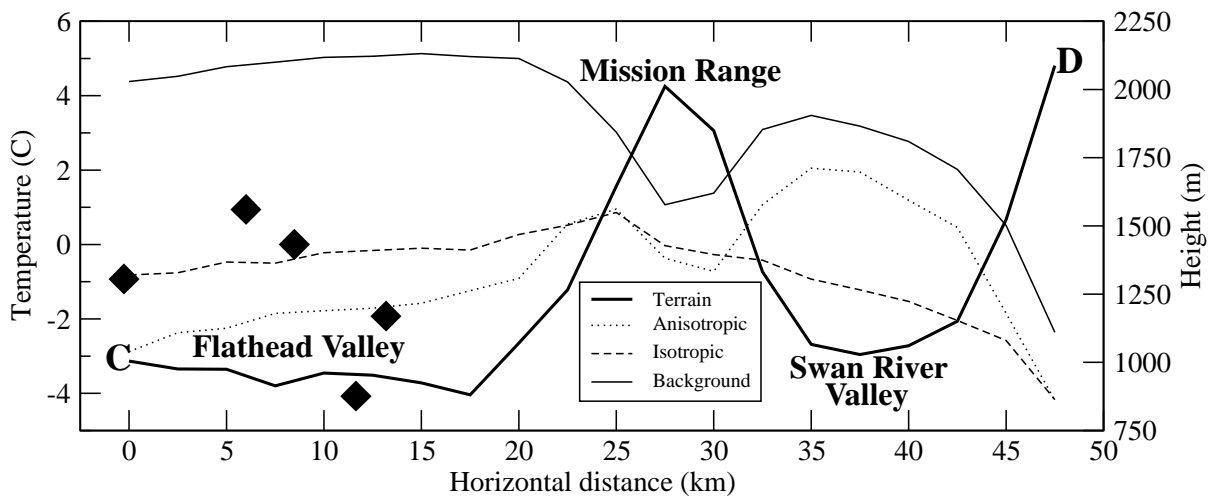


Figure 11: Same as Fig. 8 but for line segment CD in Fig. 9 at 0800 UTC 20 March 2003. Black diamonds denote temperature ($^{\circ}\text{C}$) observations located within 20 km of the cross section.